Fibers and Polymers 2020, Vol.21, No.4, 751-761
DOI 10.1007/s12221-020-9624-2

ISSN 1229-9197 (print version)
ISSN 1875-0052 (electronic version)

Water Purification Filter Prepared by Layer-by-layer Assembly of Paper Filter and Polypropylene-polyethylene Woven Fabrics Decorated with Silver Nanoparticles

Gajanan Ghodake[1], Surendra Shinde[1], Ganesh Dattatraya Saratale[2], Avinash Kadam[3], Rijuta Ganesh Saratale[3], and Dae-Young Kim[1]*

[1]*Department Biological and Environmental Science, College of Life Science and Biotechnology, Dongguk University-Seoul, Goyang 10326, Korea*
[2]*Department of Food Science and Biotechnology, Dongguk University-Seoul, Goyang 10326, Korea*
[3]*Research Institute of Biotechnology and Medical Converged Science, Dongguk University-Seoul, Goyang 10326, Korea*
(Received June 13, 2019; Revised September 17, 2019; Accepted September 23, 2019)

Abstract: Cellulose-based water filters are an affordable alternative to remove particulate matter; however, bacteria are too small to be removed simply through size exclusion. Cellulose-based water filters prepared by layer-by-layer (LBL) assembly with polypropylene-polyethylene (PP/PE) fabric decorated with silver nanoparticles (AgNPs) were tested to remove bacteria from water samples. The gallic acid reduction method was used to produce potent antibacterial AgNPs; their decoration onto PP/PE woven fabrics and the preparation of five-layered paper filters were further investigated. The use of acidic conditions for loading AgNPs and improving their spatial distribution onto the PP/PE fabrics, as revealed by scanning electron microscopy, was found to be correlated with the fabrics' antibacterial activity. The PP/PE fabrics decorated with a higher density of AgNPs (at pH 2) showed 96.7 % and 97.9 % reductions in the growth of *E. coli* and *S. aureus*, respectively. Similarly, paper filters fabricated by LBL assembly of AgNP@PP/PE fabrics with cellulose filters deactivated growing *E. coli* and *S. aureus* bacteria with good efficiency: approximately 99.4 % and 98.7 %, respectively. The results indicate that fabricating water purification filters from the cellulose-based paper is feasible with LBL type assembly. The assembled paper filters could be commercialized for point-of-use water purification in the future to prevent the spread of water-borne diseases.

Keywords: Polypropylene-polyethylene, Silver nanoparticles, Layer by layer, Paper filters, Point-of-use

Introduction

In developing countries lacking adequate water purification services, point-of-use portable tools for instant water purification are needed, especially in rural areas that lack sophisticated infrastructure. The greatest threat to humanity is bacterial contamination of water sources, which can cause outbreaks of diseases such as cholera, giardiasis, cryptosporidiosis, and gastroenteritis [1-3]. A nanosilver-silica composite with prolonged antibacterial effects was recently reported as a potential material for use in wound dressings [4]. Membrane filtration (ultrafiltration and microfiltration) has been recently adopted as a new process for the large-scale filtration of drinking water; however, the membranes suffer from easy fouling and clogging and are not affordable [5,6]. Antibacterial metal nanoparticles (silver and copper) in water filtration systems, typically in the form of coatings on steel, membranes, polymers, and filters, provide an antibacterial effect and prevent bacterial fouling [7-9]. Interest in the manufacture of nano-enabled filters for water purification has been increasing because such filters can be portable, inexpensive, lightweight, and easy to distribute and use [10,11].

Cellulose fibers are used in disposable filters, such as coffee, green tea, and dust filters. Water filters based on cellulose fibers have large pores that promote water percolation; however, they are ineffective in removing bacteria through size exclusion; modification of such techniques is, therefore, desirable to achieve a bactericidal effect. Filters, especially those made of natural fibers, are susceptible to the growth of microorganisms, which can lead to disease transmission, fouling, and reduction in the filtration rate [12].

Silver nanoparticles (AgNPs) are a potent antibacterial agent [13,14]. The aforementioned issues can be addressed by incorporating antibacterial AgNPs in a wide range of cellulosic materials such as cotton fabric, bacterial cellulose, paper filters, and cellulose gels [15-18]. A polymeric substrate called polyetheretherketone was recently coated with AgNPs using a wet chemical method at room temperature [19]. Metal nanoparticle behavior is dependent on size, shape, chemical composition, and surface charge, as well as the surrounding solution chemistry (e.g., pH and ionic strength) [20,21]. Such factors play important roles in determining the fate of nanoparticles, whether for aggregation with other nanoparticles or deposition onto given surfaces [22].

In the present study, AgNPs were prepared by the gallic acid reduction method and decorated onto the polypropylene-polyethylene (PP/PE) woven fabrics via the dip-coating technique under different pH conditions. Our approach is to embed AgNPs onto PP/PE fabrics and use for assembled

*Corresponding author: sbpkim@dongguk.edu

layer-by-layer (LBL) with cellulose filter disinfecting the drinking water contaminated with water-borne bacteria. To the best of our knowledge, this work represents the first report of the preparation and testing of AgNP@PP/PE paper filters as point-of-use water purifiers. The AgNP@PP/PE fabrics washed with DI water and used in the LBL system with cellulose filters kill bacteria through physical interaction and biocidal activity. A bacterial suspension was passed through AgNP@PP/PE paper filters, and the effluent water was analyzed to assess viable bacteria and the bactericidal effect of the AgNPs. The porosity of the paper filters enables microorganisms to contact the AgNPs; however, a strong attachment to the fiber surfaces limits the dispersal of AgNPs in the effluent water. The results revealed that the purification mechanism is the removal of bacteria from the water by filtration and deactivation of bacteria before percolation through the AgNP@PP/PE paper filter structure. The large pore size of the paper filters enables good flow by gravity, without the need for suction or pressure.

Experimental

Materials

Desiccated beef extract, Luria-Bertani (LB), nutrient broth (NB), and agar powder were purchased from Becton Chemicals Co. (Dickinson, France). Silver nitrate in grain form was purchased from Sigma-Aldrich (Germany). NaOH (1 M) stock solution (prepared in water) was obtained from Chemicals Co. (Daejung, Korea). Bacterial cultures of including *Staphylococcus aureus* (KCCM 11335; *S. aureus*) and *Escherichia coli* (KCCM 11234; *E. coli*) were obtained from the Korean Culture Center of Microorganisms (KCCM, Seoul, South Korea). Whatman paper filter (grade 113) with high strength, a pore size of 30 μm, and a thickness of 0.40 mm were acquired from Sigma-Aldrich (Sweden). The PP/PE woven fabrics manufactured with dimensions of 25×35 cm^2 for food packaging purposes were purchased from a local supplier (TNCE Electronics, Gyeonggi-do, Korea). The PP/PE fabrics had an inner core of PP and an outer layer of PE, with a PP/PE composition of 50:50 (wt%).

Nanoparticle Synthesis and Characterization

The AgNPs were produced via the biochemical reduction method using gallic acid as a stabilizer capped onto the AgNP surface, with minor modifications to the previous report [23]. In this method, the concentration of $AgNO_3$ was varied from 0.5 to 6 mM. Four milliliters of gallic acid (12.5 mM) was mixed with the appropriate amount of 20 mM $AgNO_3$. The total volume of the reaction mixture was then adjusted to 10 m*l* by addition of nanopure water. To these solutions, 50 μ*l* of NaOH solution (1 M) was added to facilitate the reduction reaction of Ag^+ to Ag^0 at ambient temperature (22-24 °C). These suspensions turned dark brown within a fraction of a minute; however, the suspensions were kept static for 12 h. The UV-vis spectra were collected using 0.05 m*l* aliquots of as-prepared AgNP solutions diluted with 0.95 m*l* of DI water; the spectra were acquired over the wavelength range from 300 to 900 nm and plotted as a function of $AgNO_3$ concentration.

Characterization

The size distribution of the AgNPs was manually measured by counting more than 300 NPs. Fourier transform infrared (FT-IR) spectra of the gallic acid and AgNPs were recorded using a Nicolet iS 50 FT-IR spectrometer with a KBr automated beam splitter. A pellet of gallic acid and AgNPs in a KBr matrix (1:100 ratio) was prepared and air-dried, and the FT-IR spectra were recorded in the wavenumber range from 500 to 4000 cm^{-1}. The crystal structures of the AgNP thin films were examined by X-ray diffraction (XRD). The XRD patterns were recorded on an X-ray diffractometer (Malvern Panalytical XPert PRO) in the range $30^\circ \leq 2\theta \leq 80^\circ$ in scanning mode using Cu Kα radiation. AgNP dispersions were deposited onto glass and dried before analysis by X-ray photoelectron spectroscopy (XPS) using a Thermo Fisher Scientific (UK) spectrometer equipped with a monochromatic Al Kα X-ray source. The XPS peak energies were calibrated against the C1s peak at 284.5 eV. Scanning electron microscopy (SEM) was used to study the morphology of the AgNPs decorated into PP/PE fabrics. Dried samples were coated with a thin layer of platinum and imaged with a Hitachi S4700 field-emission scanning electron microscopy (FE-SEM) system

AgNP-decorated PP/PE Fabrics

AgNP@PP/PE fabrics were prepared as follows. PP/PE fabrics (5 cm×5 cm) were immersed into 20 m*l* of an AgNP solution at a fixed concentration and various pH levels from 5.0 to 2.0. The PP/PE fabrics were removed gently from the AgNP solution and rinsed three times with DI water to remove excess AgNPs and avoid pH effects. Excess water was then removed by drying the AgNP@PP/PE fabrics in an oven at 40 °C for 6 h. The AgNPs coated on PP/PE fabrics were subsequently imaged by FE-SEM and characterized by XRD measurement.

Layer-by-layer Assembly

The LBL assembly method has been demonstrated to be a promising technique over the past two decades and has potential applications in the fabrication of water-purification membranes [24,25]. The LBL assembly was based on a technique described by Ottenhall *et al*. [26], where the paper filter and polyelectrolyte layers are alternated. This type of paper filter was assembled by the LBL method to introduce a portable point-of-use water filters. The difference between our method and the procedure reported by Ottenhall *et al*. is that the AgNP@PP/PE fabrics were used instead of

polyelectrolytes. Whatman paper made of cellulose was used as the paper filter. It is robust, unlike the cellulose pulp fibers used in a previous study [2]; hence, no dissolution was expected. Five layers of AgNP@PP/PE fabric were assembled in alternating fashion with layers of a paper filter, where six layers of the paper filter were required, being the first and the last layer. The AgNP@PP/PE fabrics and paper filter were prepared as a stacked LBL assembly. A paper filter was also prepared using PP/PE fabrics without modification by AgNPs and used as a control reference sample in the filtration tests. The LBL-assembled paper filters with AgNP@PP/PE fabrics were air-dried at room temperature before being used as a filter. The average weight and thickness of a single circular sheet of paper filter were approximately 70 mg and approximately 0.40 mm, respectively. Filters composed of AgNP@PP/PE fabrics and paper filters stacked in alternating fashion were installed in syringe filters.

AgNP@PP/PE Antibacterial Studies

Disk-diffusion Assay

The disk-diffusion agar method was used to test the effectiveness of the PP/PE fabrics decorated with AgNPs on Gram-positive and Gram-negative bacteria. Bacteria (*S. aureus* and *E. coli*) were spread onto an agar plate, and the seeded inoculum (CFU 104/m*l*) was allowed to dry on the plate for 20 min at 24 °C. Specimen disks of PE/PP were decorated with AgNPs at different pH (5, 4, 3, and 2) and placed on nutrient agar. *S. aureus* and *E. coli* were allowed to grow on the nutrient agar plates at 37 °C for 24 h. A zone of inhibition was then observed around the specimens. The growth-free space around every disk of AgNP@PP/PE fabrics indicated the lethality of the AgNPs toward the bacteria.

Effect on a Growth Curve

The cultures of *S. aureus* and *E. coli* were used to inoculate nutrient broth (NB) and Luria-Bertani broth (LB) media, respectively, at 1:400 dilution in the assays. The well-grown inoculum was then aliquoted into a series of culture tubes, to which AgNP@PP/PE fabrics or PP/PE specimens were subsequently added. Then, 1 m*l* of these solutions were placed into a sterilized UV-vis cuvette and banded in duplicate. The bacterial growth at 37 °C was recorded by measuring the optical density (OD) at 600 nm at 0, 3, 6, 9, 12, 24, and 32 h. The absorbance data were plotted as a function of the incubation time to assess the effect on the growth-curve phases.

Testing the Paper-filter Bactericidal Properties

The bactericidal activity of the AgNP@PP/PE paper filters was tested against *E. coli* and *S. aureus*. The bacteria grown in nutrient media were separated by centrifugation for 7 min at 3000 rpm and then suspended in peptone water and diluted to an absorption value of 0.1, which corresponds to approximately 110 colony-forming units (CFU)/m*l*. These diluted bacterial suspensions used as a model for contaminated water were passed through the filter. The water flowed gravity, enabling free-flow filtration. To test the effluent water for infiltrated bacteria, the effluent was cultured with fresh nutrient broth and bacteria suspensions were monitored at 600 nm for 24 h.

Results and Discussion

Synthesis and Characterization of AgNPs

The aqueous-phase $AgNO_3$ (0.5, 1.0, 2.0, 3.0, 4.0, 5.0, or 6.0 mM) and freshly prepared gallic acid solution were mixed such that the gallic acid concentration was 5 mM, and the resulting mixture was incubated at 22-24 °C for 12 h. The synthesis of AgNPs was initially observed by an immediate color change (within a fraction of a minute) from colorless to dark brown, which is attributed to the excitation of surface plasmon resonance (SPR) of the AgNPs, as shown in the inset of Figure 1(a). The AgNP suspensions were diluted

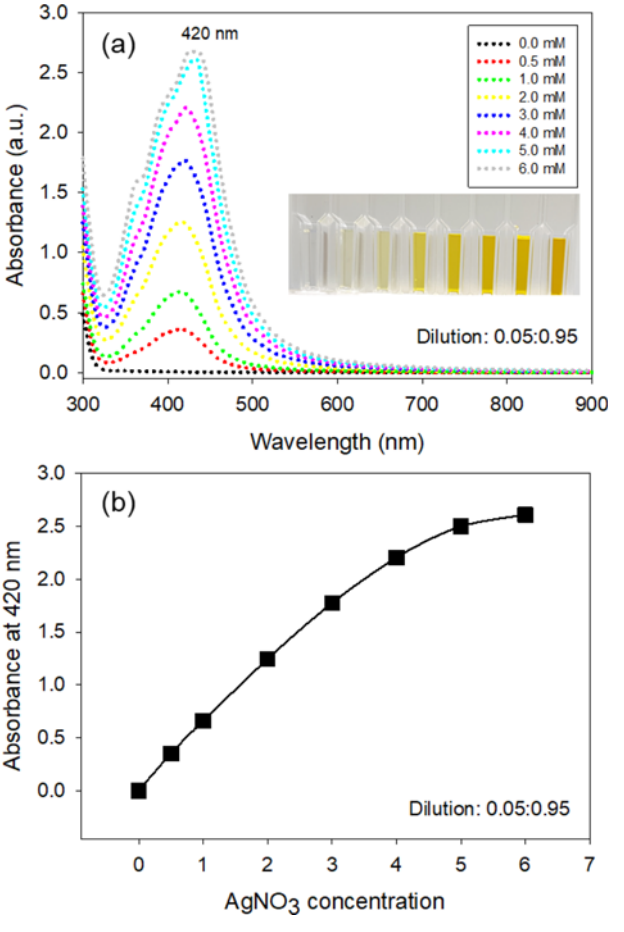

Figure 1. (a) UV-vis spectrum of AgNP suspensions obtained using increasing concentrations of $AgNO_3$ (0.5 to 6 mM) and (b) Absorbance intensity recorded at 420 nm for AgNP suspensions prepared using increasing concentrations of $AgNO_3$ (0.5 to 6 mM).

with DI water (AgNPs:H_2O 0.05:0.95 ratio). The UV-vis spectra of the AgNPs showed an absorption peak at 420 nm (Figure 1(a)), which indicates AgNPs were produced. For all of the investigated AgNPs trials, we systematically observed a progressive SPR in the extinction spectra without any red-shift, broadening, or damping of the peaks (Figure 1(a)). This trend was typical; it quantitatively depends on the $AgNO_3$ concentration without deterioration of the AgNP properties (i.e., size, shape, and molecular capping). To the best of our knowledge, a reaction mixture at pH 11 was adjusted by 50 µ*l* NaOH (1 M), where dihydroxyl group's starts two-electron oxidation reaction and it was a prerequisite to produce a high yield of the stabilized AgNPs. The oxidation of phenolic-OH groups was used to induce the formation of the quinone form, which is essential for the reduction of Ag^+ and the rapid nucleation and isotropic growth of the AgNPs as reported recently [27].

To fulfill the growing demand for AgNPs in various applications, attention toward green chemistry principles is essential to enable the easy synthesis and the formation of high-concentration suspensions of metal NPs. The brown color appeared within a fraction of a minute, confirming the compatibility of the gallic acid method with the real-time monitoring green chemistry principle (P11) "real-time monitoring and process control to prevent pollution". In addition, this method is excellent to maximize atom economy of the process; it was revealed by the transformation of 5 mM $AgNO_3$ (98.60 %) using only 5 mM gallic acid. A plot of the absorbance recorded at 420 nm as a function of the $AgNO_3$ concentration was found to be linear within the $AgNO_3$ concentration range from 0.5 to 5 mM, indicating that high-concentration suspensions of AgNPs were obtained (Figure 1(b)). Thus, the method demonstrates excellent productivity. Furthermore, the formation of well-defined AgNPs with long-term stability was observed at ambient temperatures (22-24 °C), compatible with green chemistry principles P6 'design for energy efficiency' and P3 "less hazardous chemical synthesis" [28].

The physicochemical properties of AgNPs were investigated by FT-IR, XRD, XPS, and SEM. Figure 2a shows the FT-IR spectra of both the gallic acid and the AgNPs. A broad FT-IR peak was observed in the range 3353 and 3422 cm^{-1}; were attributed to the -OH and stretching vibrations of galllic acid and AgNPs. Typically after the reaction of gallic acid with $AgNO_3$, the position of the aforementioned peak was shifted toward higher wavenumber. This evidence reveals that deprotonation of gallic acid was prerequisite to produce electron for reduction of Ag^{1+}. In agreement with the interpretation of Yoosaf *et al.*, the peak at 3422 cm^{-1} also is the good evidence of the formation of intermolecular hydrogen bonding from hydroxyl the group around the AgNPs [29]. The intensity of stretching vibration of C-O bond at 1337 cm^{-1} was retained for AgNP sample, however the intensity of bending vibration of O-H bond at 1040 cm^{-1}

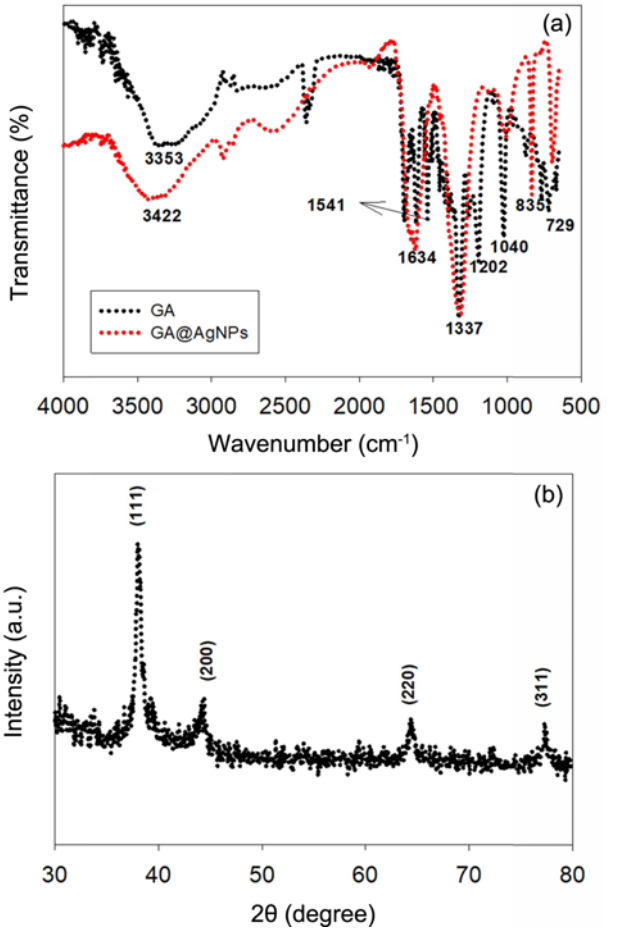

Figure 2. (a) FT-IR spectra of gallic acid and AgNPs and (b) XRD pattern of the as-prepared AgNPs.

region was clearly decreased. The FT-IR spectra observed for both gallic acid and AgNPs showed that the stretching vibration peak of carbonyl group at 1634 cm^{-1} remained identical. As observed in Figure 2(a), some of the fingerprint vibrational peaks of gallic acid at 1541 and 1202 cm^{-1} was disappeared after the formation of AgNPs, and this can be one of a clue of the oxidation of the phenolic-OH to form quinone like structure, immediately after the reduction reaction of $AgNO_3$ [27].

The XRD pattern of the obtained NPs demonstrates the formation of highly crystalline AgNPs. Characteristic XRD diffraction peaks of AgNPs at 2θ angles of 37.9°, 44.6°, 64.7°, and 77.7° correspond to diffraction of the (111), (200), (220), and (311) lattice planes of Ag, respectively (Figure 2(b)). Furthermore, the XRD patterns reveal that the AgNPs were highly crystalline, with a cubic structure [30]. Figure 3(a) shows the XPS survey scan of the AgNPs and the high-resolution Ag3d, C1s, and O1s spectra. The binding energy (BE) of AgNPs was examined by XPS to correlate the Ag3d spectra with the formation of Ag clusters. Figure

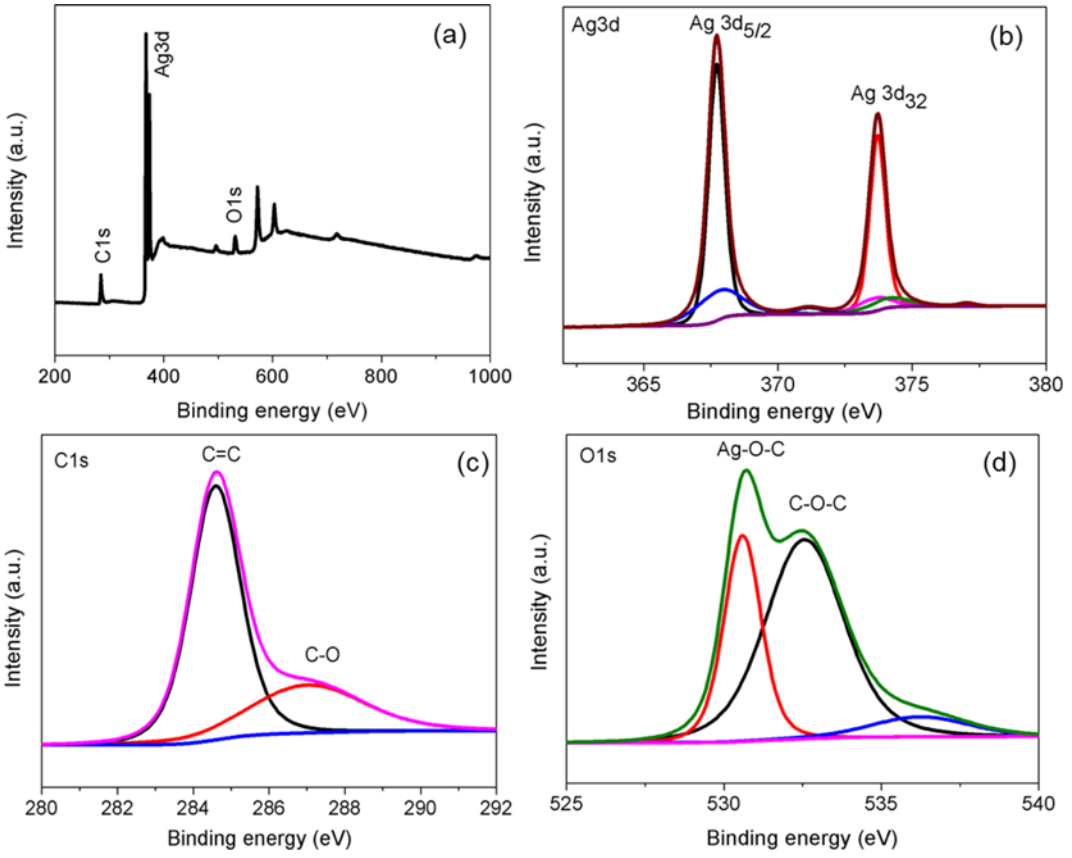

Figure 3. XPS analysis of AgNPs; (a) survey scan, (b) high-resolution Ag3d, (c) high-resolution Cls, and (d) high-resolution O1s.

3b shows two XPS peaks with BEs of 373.7 eV and 367.8 eV; these peaks are attributed to the $Ag3d_{3/2}$ and $Ag3d_{5/2}$ electrons of Ag(0), respectively, with a spin-energy split of approximately 5.9 eV. As shown in Figure 3(c) the C 1s core level resulted in two distinct components for as-prepared AgNPs. The first one appearing at the binding energy of 284.5 eV is a major peak and allocated to carbon atoms (C-C bond) within the phenyl rings of gallic acid [27]. The other peak seen in higher binding energies about 286.7 eV, is originated from to electron emission from carbon in C-O. In the XPS core-level spectra of gallic-acid-protected AgNPs, the single O1s peak at 531.2 eV is attributed to the oxygen of the hydroxyl groups (-OH), as shown in Figure 3(d). The results of the FT-IR and XPS analyses of the AgNPs are in agreement, revealing that C-O, and O-H are surface functional groups. The peak for the C-O species arises from the interactions of AgNP surfaces with the oxygen-containing functional groups of gallic acid. These groups can bond with metal surfaces, resulting in behavior through electrostatic interactions that is useful and essential for developing practical applications [31].

Characterization of AgNP@PP/PE Fabrics

The AgNPs prepared using 2 mM $AgNO_3$ at 24 °C were stored and used for characterization and deposition onto the PP/PE fabrics. A low-magnification SEM image of the PP/PE fabric is presented in Figure 4(a). To manufacture AgNP@PP/PE fabrics, the adsorption efficiency of PP/PE woven fabrics was observed for obtained AgNP solutions in different acidic environments. Micrographs of AgNPs decorated at pH 5, 4, 3, and 2 are shown in the SEM images in Figures 4(b)-(e). The AgNPs' size distribution confirms that their sizes ranged from 8 to 17 at pH 5, with an average of 13 nm, as shown in the inset of Figure 4(b). As the SEM image in Figure 4(c)-(d) shows, the AgNP aggregates were small sized and formed an identical structures and distribution over PP/PE surfaces upon treatment from pH 4 to 3. However, the AgNP aggregates were increased substantially in size and formed an excellent deposition upon treatment at pH 2, as can be seen in SEM image (Figure 4(e)). The SEM images confirmed that AgNPs were decorated onto PP/PE fabrics, suggesting that the mean diameter of the AgNPs increased with increasing acidity of the AgNP suspension (Figure 4(b)-(e)). This behavior is attributed to an increase of the zeta potential of the AgNPs, as suggested in a previous report [32]. The loading of AgNPs was achieved through multiple interactions, including hydrogen-bonding attraction, van der Waals attractions, and

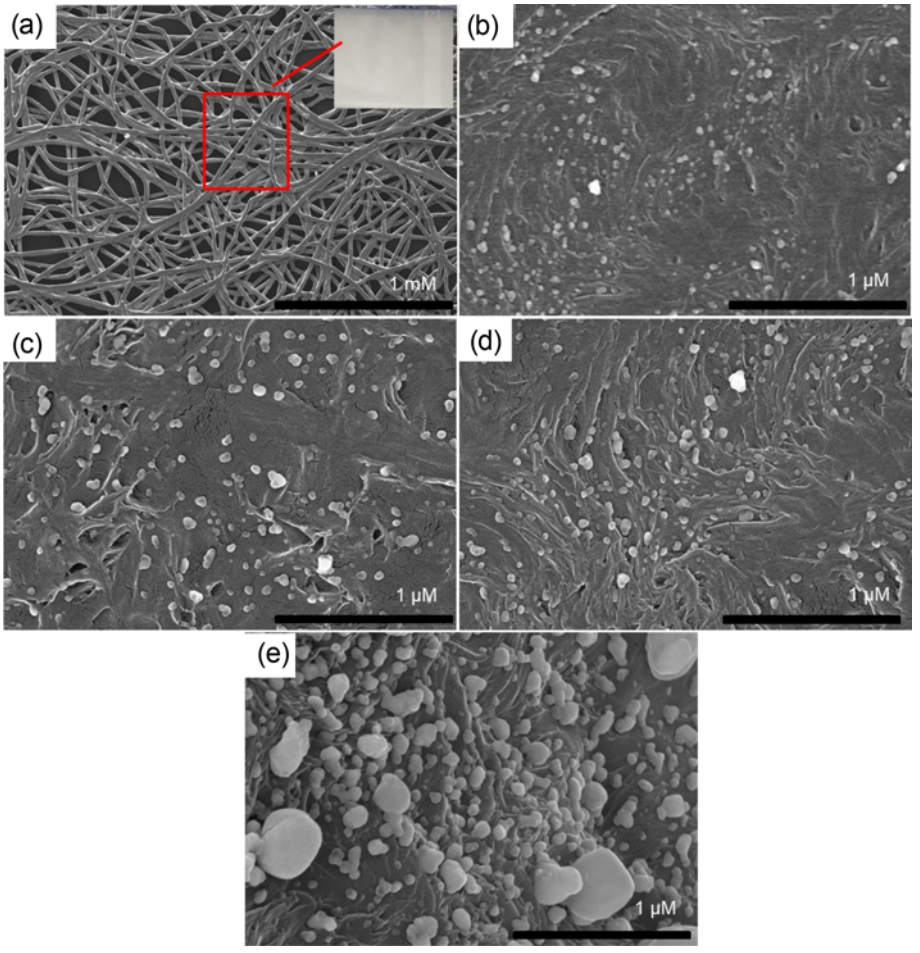

Figure 4. SEM images of (a) PP/PE woven fabrics (inset is the PP/PE fabric bag), PP/PE decorated with AgNPs prepared at pH 5, (c) PP/PE decorated with AgNPs prepared at pH 4, (d) PP/PE decorated AgNPs prepared at pH 3, and (e) PP/PE decorated AgNPs prepared at pH 2.

electrostatic attraction between AgNPs and PP/PE fabrics, similar to the observations in a previous report [33]. Improvement in the spatial distribution of AgNPs onto PP/PE fabrics should be a promising strategy in the fields of nanomedicine, water filtration, and food packaging materials [34].

The crystalline structure of the prepared AgNPs@PE/PP fabrics at different pH conditions was determined using XRD measurement and were shown in Figure 5. The identical XRD peaks observed for all tested samples can be indexed to monoclinic phase from a composite PP/PE fabrics according to the JCPDS No. 089-0032 (Figure 5). These XRD patterns are from composite of PP/PE fabrics, the reflections from PE found at 21.3° and 23.7° and for PP at 13.9°, and 16.6° and these peaks are in agreement with the previous report on PE/PP blends [35]. It can be seen from Figure 5 that the AgNPs@PP/PE fabrics prepared at pH 2 forms quite different XRD patterns compared to the other samples of PP/PE and AgNPs@PP/PE samples. The XRD pattern for the sample prepared at pH 2, clearly

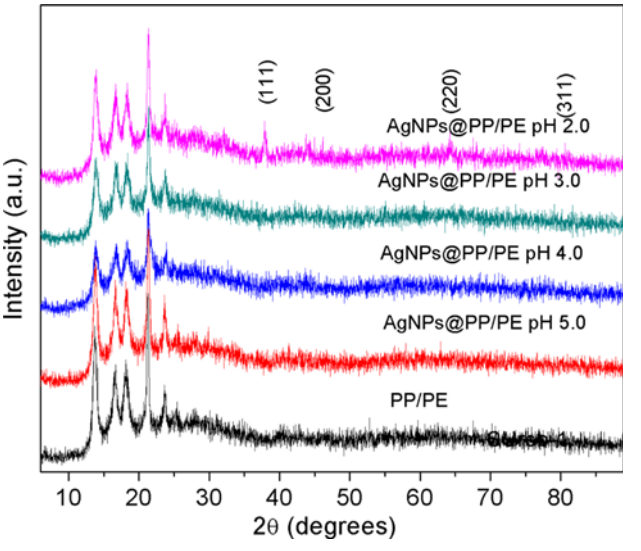

Figure 5. XRD patterns of PP/PE and AgNPs decorated PP/PE fabrics.

showed that the AgNPs were effectively decorated on PP/PE fabrics and were crystalline (Figure 5). Four different Bragg reflection peaks from the cubic structure of pure AgNPs (JCPDS, file No. 004-0783), were observed at 2θ values of 37.9°, 44.6°, 64.7°, and 77.7° which were indexed to (111), (200), ((220) and (311) planes, respectively (Figure 5), and in good agreement with previous reports on AgNPs [36-38]. The size of AgNPs decorated onto the PE/PP fabrics by pH 2 treatment was calculated by using Debye-Scherer's equation.

$$D = \frac{K\lambda}{\beta\cos\theta}$$

where D is the crystallite size, λ is the wavelength of X-ray (1.54 Å), K ~0.89, β is the full width at half maximum of the XRD peak, and θ is the Bragg's angle. The XRD peak corresponding to 37.8° was due to the AgNPs from crystal structure corresponding to the lattice plane (111). The size of deposited AgNPs has estimated about 11 nm from the breadth of the (111) reflection. The obtained value of crystallite size is attributed to the presence of non-aggregated AgNPs onto the PP/PE fabric surface with high density at pH 2.

Disc-diffusion Assay

In the first part of the present study, we systematically explored the acid-responsive nature of AgNPs and their interactions with PP/PE fabrics by adsorption, paving the way for the design of AgNP@PP/PE fabrics. Such a hybrid nanocomposite could be used as a surface protectant for waterborne pathogens, providing an alternative to traditional suspension-based biocide agents [39]. The diffusion of AgNPs within the agar medium is an important factor that defines the size of the inhibition zone. The antibacterial activities of the AgNP@ PP/PE fabrics were compared with that of pristine PP/PE fabrics. Cells of both Gram-negative bacteria (*E. coli*) and Gram-positive bacteria (*S. aureus*) were inoculated onto a nutrient agar plate with different specimens of PP/PE fabrics decorated with AgNPs. The yellow color of the respective PP/PE fabric samples is

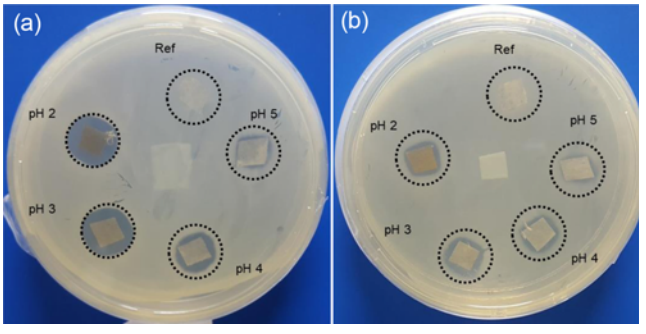

Figure 6. Zone of inhibition on nutrient agar plates containing specimens of PP/PE decorated with AgNPs prepared at different pH conditions, as labeled in the figure; (a) *S. aureus* and (b) *E. coli*.

consistent with a good distribution of AgNPs. Photographs of the AgNP@PP/PE fabrics with increasing AgNP concentrations are shown in Figure 6. The highly effective antibacterial specimens produced a wide ring due to no bacterial growth. Less effective antibacterial specimens showed no change in the surrounding bacterial colonies. The AgNP coatings formulated at pH 3 and 2 exhibited greater diffusion of AgNPs around the PP/PE fabrics, resulting in the largest inhibition zones (14 and 17 mm average values for coatings formulated at pH 3 and 2, respectively) (Figure 6(a)). The trend of the appearance of the inhibition zone is similar to the growth curve profile, as we describe in section 3.4, where a PP/PE sample treated at pH 2 shows maximum antibacterial activity against *S. aureus*. Notably, the zone of inhibition is dependent on the release of Ag^+ ions and the diffusion of AgNPs from the PP/PE fabrics, as reported previously [40,41].

The antibacterial effects of AgNP@PP/PE fabrics prepared at different pH levels were also tested against *E. coli*. The clear zones of PP/PE fabrics decorated with AgNPs against *E. coli* are demonstrated in Figure 6(b). The AgNP coatings prepared at pH 3 and 2 supported on PP/PE fabrics (Figure 6(b)) showed superior inhibition activity compared with pristine PP/PE fabrics. Thus, no colonies grew where AgNP@PP/PE fabrics allowed the diffusion of either AgNPs or Ag^+ ions into the agar. The zones of inhibition against *E. coli* cells were visible for AgNP@PP/PE fabrics prepared under pH 4, 3, or 2 (Figure 6(b)). Thus, this strategy of aggregative deposition of AgNPs onto PP/PE fabrics enables maximum biocidal activity. The greater distribution and stability of AgNPs on PP/PE fabrics may be responsible for the antimicrobial activity toward both Gram-negative, Gram-positive, and antibiotic-resistant bacteria [42].

Effect on Growth

The antibacterial activity of the AgNP@PP/PE fabrics was assessed against Gram-positive bacteria (*S. aureus*) in NB media and Gram-negative bacteria (*E. coli*) in LB media by turbidity measurements (Figure 7). The bacterial growth curve was plotted for the recorded OD of the culture suspensions vs. time. First, we investigated how *S. aureus* cells respond to AgNP@PP/PE fabrics and their potential in targeting biofilm inhibition [43]. The area under the growth curve was also observed for AgNPs decorated PP/PE woven fabrics formed by acidic pH treatment at 5, 4, 3, or 2. The OD at 600 nm indicates the number of bacterial cells; the absorbance increased in a sigmoidal fashion in the absence or with less effective AgNPs on the PP/PE fabrics produced at pH 3 and 2 (Figure 7(a)). However, for AgNPs @PP/PE fabrics produced at pH 3, the initial lag phase was extended to 12 h compared with that of the control cells; surviving bacteria growth reached a maximum within 24 h (Figure 7(a)). A further increase in the loading of AgNP aggregates

treated at pH 2 caused the complete inhibition of the growth of *S. aureus*. The absorbance ranged from 0.012 to 0.054 for 36 h (Figure 7(a)). This sample was considered to be completely inhibited, resulting in 97.9 % efficiency for *S. aureus*. Growth curve results indicated *S. aureus* cells growth can be successfully inhibited with AgNP@PP/PE fabrics, whereas pristine PP/PE fabrics did not (Figure 7). Currently, there is great interest in creating antibacterial materials or coatings with antimicrobial NPs in the context of addressing bacterial resistance [44].

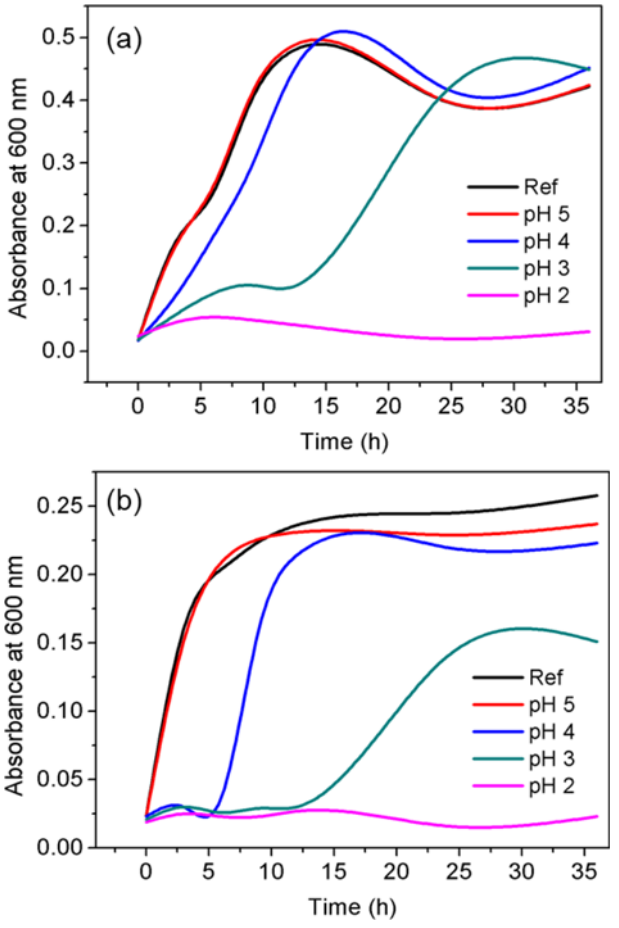

Figure 7. Effect of PP/PE decorated with AgNPs prepared at different pH conditions on the growth of bacteria in nutrient media; (a) *S. aureus* and (b) *E. coli*.

The observed effects on the growth and the lag phase of Gram-negative bacteria (*E. coli*) are shown in Figure 7(b). The growth curve plotted using absorbance vs. time indicates the density of *E. coli*; the absorbance increased in a similar sigmoidal fashion, depending on the density of AgNPs onto PP/PE fabrics. For AgNP@PP/PE fabrics produced at pH 3, the initial lag phase was successfully extended to 6 h compared with the cells grown with pristine PP/PE fabrics. However, surviving *E. coli* cells successfully continued their growth, reaching a maximum within 15 h (Figure 7(b)). Similarly, for AgNP@PP/PE fabrics formed at pH 3, the initial lag phase was effectively extended to 14 h compared with the cells grown with control samples. Surviving *E. coli* cells continued their growth, reaching a half-maximum within 35 h (Figure 7(b)). The control experiment with specimens of PP/PE fabrics showed high turbidity because of bacterial growth; by contrast, AgNP@PP/PE fabrics prepared in an acidic environment at pH 2 showed 96.7 % inhibition of the bacterial growth of *E. coli*. The pH-mediated loading of AgNPs, therefore, exhibited density-dependent antibacterial activity that inhibited visible bacterial growth. Because AgNPs are well known to demonstrate antibacterial activity, they can be used as coating materials for water filters, wound-healing bandages, and medical devices to prevent bacteria-related infections [45]. Textiles containing AgNPs have been synthesized and shown to exhibit significant antibacterial activity against *E. coli* and *S. aureus* [46].

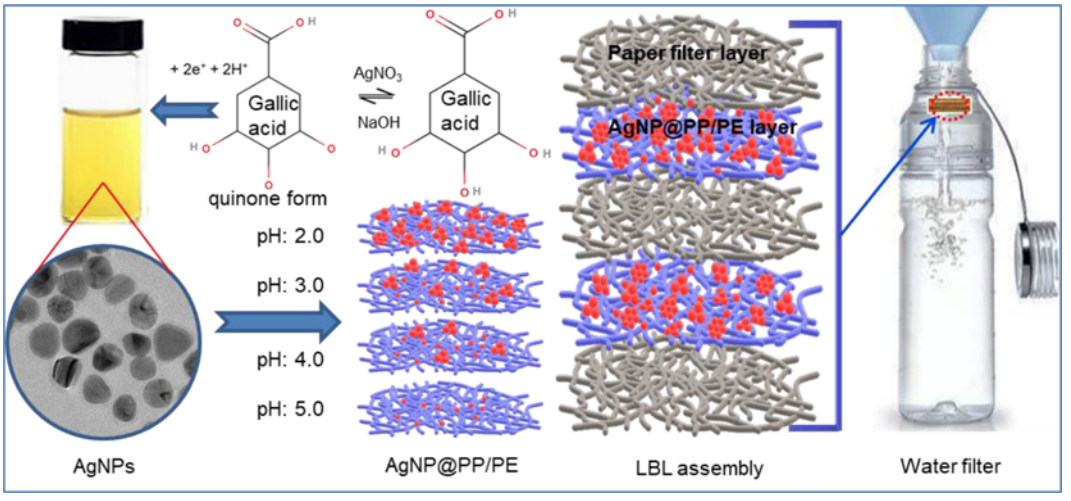

Figure 8. Schematic depicting the retention of bacteria in paper filters containing PP/PE decorated with AgNPs.

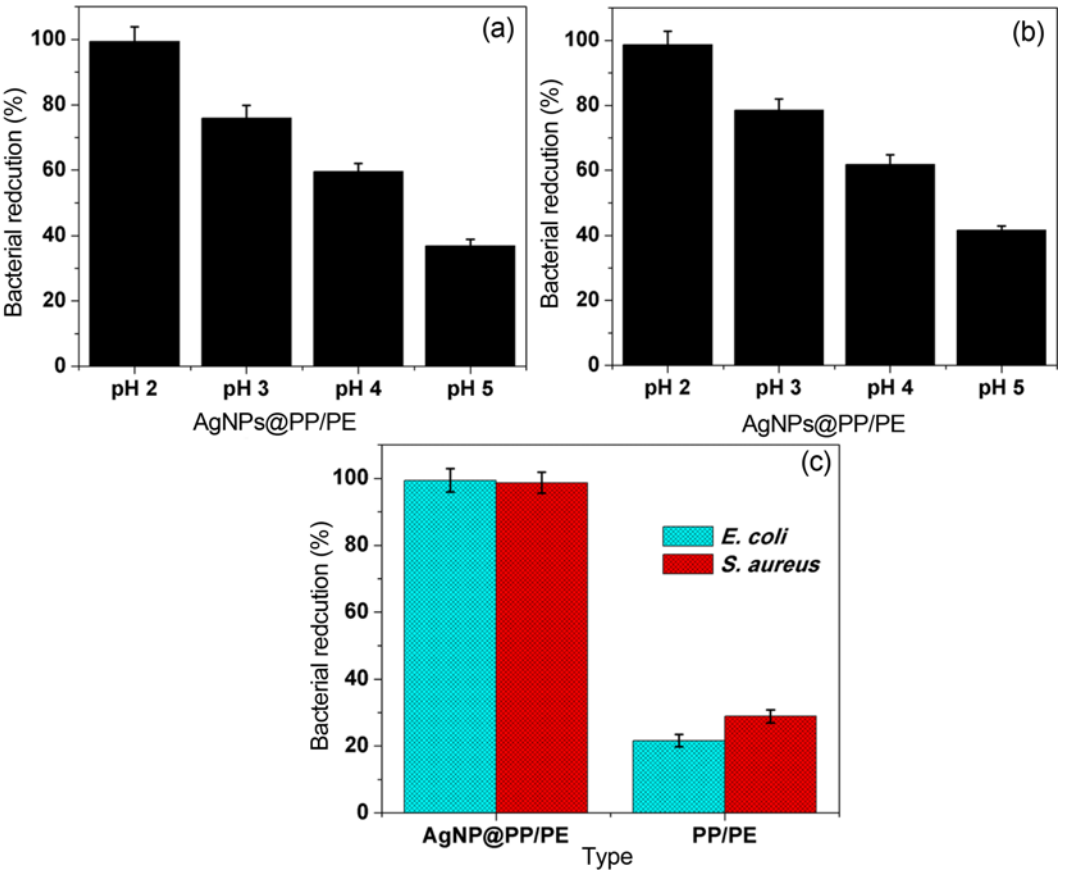

Figure 9. (a) Bacterial removal efficiency of the LBL-assembled paper filters containing PP/PE decorated with AgNPs at different pH conditions and (b) paper filter with and without AgNPs loading onto PP/PE (pH 2.0).

Bactericidal Tests for LBL Paper Filter

Most of the *E. coli* and *S. aureus* bacteria were adsorbed onto the filter, and the filtered effluents were analyzed for viability; the results confirmed that no bacteria passed through the filter (Figure 8). The test samples with five layers of assembled filter prepared at pH 5.0 removed approximately 36 and 41 % of the *E. coli* and *S. aureus* bacteria, indicating a lower loading of AgNPs on the PP/PE fabrics (Figure 9(a),(b)). The bacterial removal efficiencies of all four assemblies of paper filters were linearly dependent on the pH conditions under which the AgNP@PP/PE fabrics were prepared. The regrowth of *E. coli* in LB broth and *S. aureus* in nutrient media for filter prepared by pH 2 treatment showed the removal of approximately 99.4 % and 98.7 % of the bacteria, respectively (Figure 9(a),(b)). Thus, AgNP@PP/PE (pH 2) and paper filter provided effective and rapid removal of both *E. coli* and *S. aureus* bacteria as compared with the PP/PE and cellulose paper filter as a control reference sample (Figure 9(c)). AgNP@PP/PE fabrics prepared using the pH approaches were tested for four different pH conditions, and materials prepared at lower pH performed well because they contained the high density of AgNPs.

The use of an LBL-assembly approach for preparing the paper filter was found to be effective and rapid in removing both Gram-positive and Gram-negative bacteria from contaminated waters. The developed filters could be reused several times, and most of the *E. coli* and *S. aureus* bacteria get trapped onto the AgNP@PP/PE fabrics in the uppermost layer of the LBL assembled filter. The use of LBL assembly to induce bacteria adsorption onto AgNP@PP/PE surfaces is an interesting and promising system that could be commercialized to fabricate point-of-use water filters in the future. Further research is needed to improve the filters and the filtration design to achieve the standard recommended by the World Health Organization for water treatment and potential applications in the removal of pathogens of all classes.

Conclusion

We investigated the bacterial removal efficiency of paper filters prepared by LBL assembly of AgNP@PP/PE woven fabrics and cellulose paper filters. The bacterial reduction increased with decreasing pH used to prepare AgNPs decorated onto PP/PE fabrics, and most of the bacteria were

easily trapped in the top layers of the filter. The developed paper filters are affordable, environmentally friendly, disposable, and effective against human pathogens (*E. coli* and *S. aureus*). The antibacterial action of the LBL-assembled paper filters is based on physical adsorption and detoxification of bacteria from water without loss of AgNPs into the water because cellulose provides a supplementary surface in the paper filter. Compared with conventional water treatment options or chlorine for decontamination, the developed paper filter has an advantage in terms of the contact-active bactericidal action. The results showed potential for manufacturing portable water purification filters using the LBL assembly approach. Thus, such filters could perhaps be used for point-of-use water purification, e.g., in emergencies to prevent bacterial diseases.

Acknowledgment

This work was supported by the Dongguk University Research Fund of 2018-2020.

References

1. F. Y. Ramírez-Castillo, A. Loera-Muro, M. Jacques, P. Garneau, F. J. Avelar-González, J. Harel, and A. L. Guerrero-Barrera, *Pathogens*, **4**, 307 (2015).
2. J. Illergård, L. Wågberg, and M. Ek, *Colloid Surf. B: Biointerfaces*, **88**, 115 (2011).
3. A. W. Bivins, T. Sumner, E. Kumpel, G. Howard, O. Cumming, I. Ross, K. Nelson, and J. Brown, *Environ. Sci. Technol.*, **51**, 7542 (2017).
4. D. A. Mosselhy, H. Granbohm, U. Hynönen, Y. Ge, A. Palva, K. Nordström, and S.-P. Hannula, *Nanomaterials*, **7**, 261 (2017).
5. K. J. Howe and M. M. Clark, *Environ. Sci. Technol.,* **36**, 3571 (2002).
6. B. P. Tripathi, N. C. Dubey, and M. Stamm, *J. Haz. Mater.*, **252-253**, 401 (2013).
7. S. Afkham, A. Aroujalian, and A. Raisi, *RSC Adv.*, **6**, 108113 (2016).
8. S. M. Praveena, L. S. Han, L. T. L. Than, and A. Z. Aris, *J. Exp. Nanosc.*, **11**, 1307 (2016).
9. M. A. Ur Rehman, S. Ferraris, W. H. Goldmann, S. Perero, F. E. Bastan, Q. Nawaz, G. G. D. Confiengo, M. Ferraris, and A. R. Boccaccini, *ACS Appl. Mater. Interfaces,* **9**, 32489 (2017).
10. L. Mpenyana-Monyatsi, N. H. Mthombeni, M. S. Onyango, and M. N. B. Momba, *Int. J. Environ. Res. Pub. Heal.*, **9**, 244 (2012).
11. W.-L. Chou, D.-G. Yu, and M.-C. Yang, *Polym. Adv. Technol.,* **16**, 600 (2005).
12. A. Khoddami, S. S. Shokohi, M. Morshed, and D. Abedi, *Fiber. Polym.*, **12**, 635 (2011).
13. M. Venkataraman, R. Mishra, V. Subramaniam, A. Gnanamani, and T. S. Subha, *Fiber. Polym.*, **15**, 510 (2014).
14. X. Yue, H. Lin, T. Yan, D. Zhang, H. Lin, and Y. Chen, *Fiber. Polym.*, **15**, 716 (2014).
15. A. M. Ferraria, S. Boufi, N. Battaglini, A. M. Botelho do Rego, and M. ReiVilar, *Langmuir*, **26**, 1996 (2010).
16. F. Tang, L. Zhang, Z. Zhang, Z. Cheng, and X. Zhu, *J. Macromol. Sci. A*, **46**, 989 (2009).
17. C. Zhu, J. Xue, and J. He, *J. Nanosci. Nanotechnol.*, **9**, 3067 (2009).
18. D. Arif, M. B. K. Niazi, N. Ul-Haq, M. N. Anwar, and E. Hashmi, *Fiber. Polym.*, **16**, 1519 (2015).
19. A. F. Cruz-Pacheco, D. T. Muñoz-Castiblanco, J. A. Gómez Cuaspud, L. Paredes-Madrid, C. A. Parra Vargas, J. J. Martínez Zambrano, and C. A. Palacio Gómez, *Coatings*, **9**, 91 (2019).
20. C. Pfeiffer, C. Rehbock, D. Hühn, C. Carrillo-Carrion, D. J. d. Aberasturi, V. Merk, S. Barcikowski, and W. J. Parak, *J. Royal Soc. Interface,* **11**, 20130931 (2014).
21. C. Peng, W. Zhang, H. Gao, Y. Li, X. Tong, K. Li, X. Zhu, Y. Wang, and Y. Chen, *Nanomaterials*, **7**, 21 (2017).
22. A. R. Petosa, D. P. Jaisi, I. R. Quevedo, M. Elimelech, and N. Tufenkji, *Environ. Sci. Technol.*, **44**, 6532 (2010).
23. D. Li, Z. Liu, Y. Yuan, Y. Liu, and F. Niu, *Process Biochem.*, **50**, 357 (2015).
24. O. Sanyal and I. Lee, *J. Nanosci. Nanotechnol.*, **14**, 2178 (2014).
25. C. Picart, J. Mutterer, L. Richert, Y. Luo, G. D. Prestwich, P. Schaaf, J.-C. Voegel, and P. Lavalle, *Proc. Natl. Acad. Sci. USA*, **99**, 12531 (2002).
26. A. Ottenhall, J. Henschen, J. Illergård, and M. Ek, *Environ. Sci-Wat. Res. Technol.,* **4**, 2070 (2018).
27. M. Farrokhnia, S. Karimi, and S. Askarian, *ACS Sustain. Chem. Eng.*, **7**, 6672 (2019).
28. J. A. Dahl, B. L. S. Maddux, and J. E. Hutchison, *Chem. Rev.*, **107**, 2228 (2007).
29. K. Yoosaf, B. I. Ipe, C. H. Suresh, and K. G. Thomas, *J. Phys. Chem. C.,* **111**, 12839 (2007).
30. S. Kalathil, J. Lee, and M. H. Cho, *Green Chem.*, **13**, 1482 (2011).
31. A. Gupta, R. F. Landis, and V. M. Rotello, *Food Res.*, **5**, 364 (2016).
32. I. Ostolska and M. Wiśniewska, *Colloid Polym. Sci.*, **292**, 2453 (2014).
33. G. A. Rance and A. N. Khlobystov, *Phys. Chem. Chem. Phys.*, **12**, 10775 (2010).
34. Z. Shen, W. Baker, H. Ye, and Y. Li, *Nanoscale*, **11**, 7371 (2019).
35. T. Furukawa, H. Sato, Y. Kita, K. Matsukawa, H. Yamaguchi, S. Ochiai, H. W. Siesler, and Y. Ozaki, *Polym. J.*, **38**, 1127 (2006).
36. V. M. Kariuki, I. Yazgan, A. Akgul, A. Kowal, M. Parlinska, and O. A. Sadik, *Environ. Sci. Nano.*, **2**, 518 (2015).
37. E. Parthiban, N. Manivannan, R. Ramanibai, and N. Mathivanan, *Biotechnol. Reports.*, **21**, 297 (2019).

38. V. R. Netala, V. S. Kotakadi, L. Domdi, S. A. Gaddam, P. Bobbu, S. K. Venkata, S. B. Ghosh, and V. Tartte, *Appl. Nanosci.*, **6**, 475 (2016).
39. G. E. Machado, A. M. Pereyra, V. G. Rosato, M. S. Moreno, and E. I. Basaldella, *Mater. Sci. Eng. C.,* **98**, 789 (2019).
40. S. P. Deshmukh, S. M. Patil, S. B. Mullani, and S. D. Delekar, *Mater. Sci. Eng. C.,* **97**, 954 (2019).
41. Y. Su, L. Zhao, F. Meng, Q. Wang, Y. Yao, and J. Luo, *Colloids Surf. B: Biointerfaces*, **152**, 238 (2017).
42. S. M. Navarro Gallón, E. Alpaslan, M. Wang, P. Larese-Casanova, M. E. Londoño, L. Atehortúa, J. J. Pavón, and T. J. Webster, *Mater. Sci. Eng. C.*, **99**, 685 (2019).
43. N. Singh, J. Rajwade, and K. M. Paknikar, *Colloids Surf. B: Biointerfaces*, **175**, 487 (2019).
44. D. Campoccia, L. Montanaro, and C. R. Arciola, *Biomaterials*, **34**, 8533 (2013).
45. D. M. Eby, H. R. Luckarift, and G. R. Johnson, *ACS Appl. Mater. Interfaces*, **1**, 1553 (2009).
46. A. Azadbakht and A. R. Abbasi, *Fiber. Polym.*, **13**, 264 (2012).